THERMAL EFFECTS OF AIRFLOWS AND MOISTURE ON EXTERIOR WALL STRUCTURES

R. Kohonen

ABSTRACT

During the last ten years, extensive research work has been carried out in Finland in order to get a better understanding of the phenomena affecting the thermal performance of exterior building envelopes. This paper concerns the thermal effects of airflows. Some aspects of the influence of moisture and moisture transfer on the thermal performance of a structure will also be discussed.

Two different principles of airflows can be distingished in building structure systems: interstitial and infiltration airflows. It is well known from Bankvall's results, at which conditions interstitial natural-convection flows cause extra heat transfer in a closed space filled with fibrous insulating material. The corresponding Nu-Ra* dependency for cavities with open / permeable cold surface is given. According to the computer simulations, a structure with wind shield having permeability less than 10^{-12} behaves thermally like an enclosure. Furthermore, if horizontal convection obstructions are used, they should be thermally well conductive.

In heat-demand calculations, it is commonly assumed that infiltrating air flows into room air at the outdoor temperature. In fact, according to our computer simulations, infiltrating air warms up due to the heat transfer between infiltrating air and wall structure on the leakage route. For typical leakage routes, Nusselt numbers are 0.6 - 0.8 , which means that the heating load of infiltration air and transmission is commonly overestimated in the room air heat balance calculations. An equation to take into account the interaction-action of airflows and conductive heat transfer in structures is suggested.

The thermal performance of wall structures is influenced by moisture transfer in three ways: stagnant moisture (water) has much higher thermal conductivity than dry / humid air; moisture flows in liquid / gas phases mean convective heat transfer; interstitial phase changes also cause extra heat transfer in relation to pure conductive heat transfer. For analyzing these phenomena, a mathematical / physical modeling of simultaneous coupled heat and mass transfer in porous materials based on the volume averaging technique is discussed. In addition, some experimental results of field studies concerning the thermal performance of stuctures, where also moisture transfer occurs.

INTRODUCTION

Coupled heat and mass transfer in porous media occur in many technical systems. In building physics applications, the transport phenomena are mostly transient and coupled. For example, in exterior wall structures, transient coupled diffusive and convective heat and moisture transfer process occurs owing to time-dependent boundary conditions and drying / wetting process.

This paper concerns the thermal effects of air flows and moisture on the thermal performance of wall structures. Both simulations and experiments have been carried out. The derivation of model equations using the volume averaging approach is given to show, how the coupling of heat and mass transfer is formed.

The basic theory of simultaneous heat and mass transfer in porous media was introduced by Luikov (1961). After that a number of mathematical models based on different scientific

approaches were introduced (Lampinen 1979 ; Kiessl 1983 ; Dinuleschu 1980 ; Kohonen 1984). In every model there are parameters to be determined experimentally. The measuring methods of transport parameters are also discussed by Kiessl and Kohonen. A special problem with transport properties is the determination of the thermal conductivity of moist porous materials. This will be discussed later. Although heat and moisture transfer phenomena in building structures have been studied for a relatively long time, only a few simulation methods have been introduced (Kiessl 1983; Kohonen, Määttä 1981; Sandberg 1973).

When considering the validity of a simulation method, we should pay attention especially to the physical model, the combination of transport phenomena included in the mathematic model, transport properties, and experimental verification of the model.

In the volume-averaging approach also used in our simulation method, TRATMO, moist porous materials are considered as multiphase systems consisting of solid matrix, moisture in voids, and inert gas. Consequently, we have a mixture of three components, two inert components (inert gas in voids and solid matrix) and moisture (adsorbate) in three phases (solid like surface adsorbent, capillary condensate, and water vapor). A somewhat simplified description of the wetting process would be as follows: at first, at low water vapor pressures when physical adsorption occurs, a mono-molecular layer is formed and, when the pressure of adsorbate is increased, the layer grows into a film. Thus the system consists of two phases (solid matrix with solid-like liquid film and gas) and two components (adsorbate and adsorbent). When the pressure of adsorbate is further increased, capillary condensation is possible. Depending on the nature of the chemical potential of the absorbed film, the film may either grow monotonously into a volume phase or have a certain thickness, at which the equilibrium with the volume phases (capillary condensate and adsorbate) will be reached. Accordingly, it is obvious that the capillary condensate will freeze first when the temperature is lowered below the freezing point of free water, while the surface adsorbent will remain unfrozen. Due to heteroporosity, there is no exact freezing or evaporating point for the water in porous materials. Thus the rate of interstitial phase changes depends on the temperature and moisture content and is not constant as often assumed in Luikov's model. Figure 1 illustrates a physical model for moisture transfer in porous media.

GOVERNING EQUATIONS OF HEAT AND MASS TRANSFER IN POROUS MEDIA

The basic transport equations of any flow system are continuity, momentum, and energy. In multiphase systems, the control volume, V, consists of subvolumes, V_α, bound by time-dependent surfaces, $\partial V_\alpha(t)$, which may include interfacial and phase-intrinsic parts (Figure 2). The fact that the phase-intrinsic surfaces may be time-dependent must be taken into account on the derivation of the balance equations. According to Leibnitz's rule, we may write for the average of time derivative

$$\frac{1}{V}\int_{V_\alpha(t)} \frac{\partial \psi_\alpha}{\partial t}(V_\alpha,t)\, dV = \frac{\partial \langle \psi_\alpha \rangle}{\partial t} - \frac{1}{V}\sum_\beta \int_{\partial V_{\alpha\beta}} \psi_\alpha \vec{w}_{\alpha\beta}\cdot\vec{n}_{\alpha\beta} dA. \qquad (1)$$

Correspondingly, according to the volume-averaging theorem introduced by Slattery (1971), it holds for any scalar, spatial vector, or second-order tensor field that

$$\frac{1}{V}\int_{V_\alpha(t)} \nabla\psi_\alpha(V_\alpha,t)\, dV = \nabla\langle\psi_\alpha\rangle + \frac{1}{V}\sum_\beta \int_{\partial V_{\alpha\beta}} \psi_\alpha \vec{n}_\alpha\, dA. \qquad (2)$$

When applying Equations 1 and 2 to the general transport equation valid for single-phase systems, the general transport equation valid for a component of a multiphase system is obtained by:

$$\frac{\partial}{\partial t}\langle \rho_\alpha \psi_\alpha \rangle = -\nabla\cdot\langle \vec{q}_{eff}\rangle - \nabla\cdot\langle \psi_\alpha \vec{q}_{m,\alpha}\rangle - \frac{1}{V}\sum_\beta \int_{\partial V_{\alpha\beta}} \vec{q}_{eff}\cdot\vec{n}_{\alpha\beta}\, dA$$

$$- \frac{1}{V}\sum_\beta \int_{\partial V_{\alpha\beta}} (\psi_\alpha\rho_\alpha)(\vec{v}_\alpha - \vec{w}_{\alpha\beta})\cdot\vec{n}_{\alpha\beta}\, dA + \langle \dot{\psi}_\alpha \rangle . \qquad (3)$$

The area integrals on the right-hand side of Equation 3 describe mass, stress, inertia, or energy transfer from component α to component β across the interfacial surface $\partial V_{\alpha\beta}$, when no accumulation takes place at the interface. $\langle \Psi_\alpha \rangle$ denotes sources / sinks in the control volume.

Furthermore, we should note that if the value of the function Ψ_α in any point in phase α can be expressed $\Psi_\alpha = \langle \Psi_\alpha \rangle^{(\alpha)} + \tilde{\Psi}_\alpha$, where $\tilde{\Psi}_\alpha$ denotes spatial turbulence, then (Gray 1975):

$$\langle \Omega_\alpha \Psi_\alpha \rangle = \langle \Omega_\alpha \rangle^{(\alpha)} \langle \Psi_\alpha \rangle + \langle \tilde{\Omega}_\alpha \tilde{\Psi}_\alpha \rangle . \tag{4}$$

In continuity equation $\Psi = 1$ and if local thermodynamic equilibrium is assumed and the surface integral on the right-hand side of Equation 3 is considered as the volumetric rate of the interstitial phase changes, then

$$\frac{\partial}{\partial t} \langle \rho_\alpha \rangle = -\nabla \cdot \langle \vec{q}_{m,\alpha} + \vec{q}_{eff,\alpha} \rangle + \sum_\beta \langle \dot{q}_{m,\alpha\beta} \rangle . \tag{5}$$

In Equation 5 $\vec{q}_{eff,\alpha}$ and $\vec{q}_{m,\alpha}$ denote diffusion and convective mass flux, respectively.

Application of the volume-averaging theorem in momentum equation gives ($\Psi = \vec{v}$ and $\vec{q}_{eff} = \underline{t}$ in Equation 3) :

$$\frac{\partial}{\partial t} \langle \rho_\alpha \vec{v}_\alpha \rangle = -\nabla \cdot \langle \rho_\alpha \vec{v}_\alpha \vec{v}_\alpha \rangle + \nabla \cdot \langle \underline{t}_\alpha \rangle + \langle \rho_\alpha \vec{f}_\alpha \rangle +$$

$$+ \frac{1}{V} \int_{\partial V_\alpha} \underline{t}_\alpha \cdot \vec{n}_\alpha \, dA - \frac{1}{V} \sum_\beta \int_{\partial V_{\alpha\beta}} \rho_\alpha \vec{v}_\alpha \cdot (\vec{v}_\alpha - \vec{w}_{\alpha\beta}) \cdot \vec{n}_{\alpha\beta} \, dA. \tag{6}$$

If the modified Peclet number $Pe^* < 5$, the inertia terms in Equation 6 can be neglected (Bear 1972). When pure stratified flows are considered, the first surface integral term on the right-hand side of Equation 6 describing stress and inertia transfer can be readily integrated. Since $\underline{t}_\alpha = -p_\alpha \underline{i} + \underline{\tau}_\alpha$ the equation of motion becomes

$$\nabla \langle p_\alpha \rangle = -\nabla \cdot \langle \underline{\tau}_\alpha \rangle - \frac{1}{V} \sum_\beta \int_{\partial V_{\alpha\beta}} \underline{t}_\alpha \cdot \vec{n}_{\alpha\beta} \, dA - \langle \rho_\alpha \rangle \vec{f}_\alpha , \tag{7}$$

where

p_α is the static pressure of fluid α.

In building physical stratified viscous flows, $\nabla \cdot \langle \tau_\alpha \rangle$ is obviously of minor importance. The second term on the right-hand side of Equation 6 represents the force resisting the flow, for which a linear dependence on the relative velocity is valid (Darcy-type flow), if $Da < 10^{-3}$

$$\frac{1}{V} \sum_\beta \int_{\partial V_{\alpha\beta}} \underline{\tau}_\alpha \cdot \vec{n}_{\alpha\beta} \, dA = -\sum_\beta \eta_\alpha \cdot \underline{B}_{\alpha\beta} \cdot (\langle \vec{v}_\alpha \rangle - \langle \vec{v}_\beta \rangle) . \tag{8}$$

If $|\langle \vec{v}_\alpha \rangle| >> |\langle \vec{v}_\beta \rangle|$, then

$$\langle \vec{v}_\alpha \rangle = -\frac{\underline{K}_{v,\alpha}}{\eta_\alpha} \cdot (\nabla \langle p_\alpha \rangle^{(\alpha)} - \langle \rho_\alpha \rangle^{(\alpha)} \vec{f}_\alpha) . \tag{9}$$

As stated, Equation 9 is valid in building physical applications for pure stratified flows of bulk phases. e.g., for viscous flow of humid air and viscous or capillary flows of liquid water.

The energy balance equation in building physics applications may be presented by the isochoric change rate of internal energy ($\Psi = h$ and $\vec{q}_{eff} = \vec{q}$ in Equation 3)

$$\int_V \frac{\partial}{\partial t} (\rho_\alpha h_\alpha)\, dV = - \int_{\partial V} \vec{q}_\alpha \cdot \vec{n}_\alpha \, dA - \int_{\partial V} (\vec{q}_{m,\alpha} h_\alpha) \cdot \vec{n}_\alpha \, dA . \qquad (10)$$

Applying the divergence and volume-averaging theorems and taking into account Equation 5 we obtain

$$\frac{\partial}{\partial t} \langle \rho_\alpha h_\alpha \rangle = - \nabla \langle \vec{q}_\alpha \rangle - \nabla \cdot \langle h \vec{q}_{m,\alpha} \rangle + \langle h_\alpha \sum_\beta \langle \dot{q}_{\alpha\beta} \rangle \rangle . \qquad (11)$$

The total mass and energy balance equations for a system consisting of components α is obtained by summing together the corresponding equations valid for component α:

$$\frac{\partial}{\partial t} \sum_\alpha \langle \rho_\alpha \rangle = -\nabla \cdot \langle \vec{q}_{D,\alpha} \rangle - \nabla \cdot \langle \vec{q}_{m,\alpha} \rangle \qquad (12)$$

$$\frac{\partial}{\partial t} \sum_\alpha \langle \rho_\alpha h_\alpha \rangle = -\nabla \cdot \sum_\alpha \langle \vec{q}_\alpha \rangle + \sum_{\alpha \neq \beta}^{(\alpha)} \langle h_\alpha \rangle \sum_\beta \langle \dot{q}_{m,\alpha\beta} \rangle - \sum_\alpha \nabla \cdot \langle h_\alpha \vec{q}_{m,\alpha} \rangle . \qquad (13)$$

The left-hand side of Equation 13 represents accumulation of heat; the first term on on the right-hand side, conduction; the second, generation of heat due to interstitial phase changes; and the last term, convective heat transfer due to viscous flows. By solving $\langle \dot{q}_{\alpha\beta} \rangle$ from the continuity equation and assuming that only the phase change $\alpha\beta$ occurs in a certain temperature region, we find for the energy equation

$$\sum_\alpha \langle \rho_\alpha \rangle c_{p\alpha} \frac{\partial \langle T \rangle}{\partial t} + \ell_{\alpha\beta} \frac{\partial \langle \rho_\alpha \rangle}{\partial t} = -\nabla \cdot \langle \vec{q} \rangle - \ell_{\alpha\beta} \nabla \cdot \langle \vec{q}_{m,\alpha} + q_{D,\alpha} \rangle$$

$$\sum_\alpha \nabla \cdot \langle h_\alpha \vec{q}_{m,\alpha} \rangle . \qquad (14)$$

Equations 12 and 13 will have different forms with different boundary conditions depending on which heat and mass transfer modes are occuring, e.g., on the problem considered. Kohonen and Määttä (1981) have introduced a computer program, TRATMO, based on Equations 12 and 13 for transient analysis of the hygrothermal behavior of building structures. Methods for the determination of the transport properties and potentials needed for the calculation of viscous, diffusive, and capillary flows in Equations 12 and 13 are discussed by Kohonen (1984).

In the following, two specific topics of coupled heat and mass transfer phenomena in building structures will be discussed: steady-state combined conductive and convective heat transfer in two-dimensional structures and the influence of moisture on the thermal performance of structures.

CONVECTIVE HEAT TRANSFER IN STRUCTURES WITH PERMEABLE MATERIALS

Governing Equations

We must deal with combined conductive and convective heat transfer, in many technical systems, especially in thermal insulation. Thermal effects of natural convection flows in closed filled cavities with different kinds of boundary conditions have been studied extensively. In building physics applications, however, we deal with cavities whose envelope is more or less permeable.

Consider a two-dimensional wall structure with no interstitial phase changes. The general continuity, momentum, and energy balance equation of a multiphase system, Equations 5, 6, and 13, will have the following forms, if stationary conditions are assumed:

$$\nabla\cdot\langle\vec{q}_{m,\alpha}\rangle = 0 \tag{15}$$

$$-\nabla\cdot\langle\rho_\alpha\vec{v}_\alpha\cdot\vec{v}_\alpha\rangle + \nabla\cdot\langle\underline{t}_\alpha\rangle + \langle\rho_\alpha\vec{f}_\alpha\rangle + \frac{1}{V}\int_{\partial V_\alpha}\underline{t}_\alpha\cdot\vec{n}_\alpha\, dA = 0 \tag{16}$$

$$-\nabla\cdot\langle\vec{q}_\alpha\rangle - \nabla\cdot\langle h_\alpha\vec{q}_{m,\alpha}\rangle = 0\,. \tag{17}$$

If we assume that viscous flow is incompressible, then we have $\nabla\cdot\vec{v}_\alpha = 0$. The momentum equation will have different forms depending on the nature of viscous flow. In building physics application, it is often valid to assume a Darcy-type flow

$$\frac{1}{V}\int_{\partial V_\alpha}\underline{t}_\alpha\cdot\vec{n}_\alpha\, dA = -\underline{B}_\alpha\eta_\alpha\langle\vec{v}_\alpha\rangle = -\underline{K}^{-1}_{v,\alpha}\eta_\alpha\langle\vec{v}_\alpha\rangle \tag{18}$$

$$\nabla\cdot\langle\underline{t}_\alpha\rangle = \nabla\langle p_\alpha\rangle^{(\alpha)}, \text{ e.g., internal momentum transfer is zero} \tag{19}$$

$$\nabla\cdot\langle\rho_\alpha\vec{v}_\alpha\cdot\vec{v}_\alpha\rangle = 0, \text{ e.g., inertia transfer is zero.} \tag{20}$$

Consequently,

$$\langle\vec{v}_\alpha\rangle = -\frac{\underline{K}_{v,\alpha}}{\eta_\alpha}\cdot\left(\nabla\langle p\rangle^{(\alpha)}_\alpha - \langle\rho_\alpha\rangle^{(\alpha)}\vec{f}_\alpha\right). \tag{21}$$

If we assume that the density of fluid is a function of temperature, substitute the equation of motion, Equation 21, to the continuity equation, Equation 15, then we have

$$\frac{\underline{K}_{v,\alpha}}{\eta_\alpha}\left[\nabla^2\langle p_\alpha\rangle^{(\alpha)} - \frac{d\langle\rho_\alpha\rangle^{(\alpha)}}{dT}\vec{f}_\alpha\cdot\nabla\langle T\rangle\right] = 0\,. \tag{22}$$

Further, assuming that the fluid and solid matrix have equal temperatures locally, we may write

$$\nabla\cdot(\underline{K}_q\cdot\nabla\langle T\rangle) - \langle\vec{q}_{m,\alpha}\rangle\cdot\nabla\langle h_\alpha\rangle^{(\alpha)} = 0\,. \tag{23}$$

Equations 21 and 23 are the model equations describing combined forced / natural convection and combined conduction and convection of heat at stationary conditions.

In building physics applications, the body force $\vec{f}$ may be replaced by gravity force $\vec{g}$. If the fluid is air and is assumed to behave as ideal gas, then Equation 22 is

$$\frac{\underline{K}_{v,\alpha}}{\eta_\alpha}\left\{\nabla^2\langle p_\alpha\rangle^{(\alpha)} + \beta\langle\rho_\alpha\rangle^{(\alpha)}_{ref}\vec{g}\cdot\nabla\langle T\rangle\right\} = 0 \tag{24}$$

where

β is thermal expansion coefficient, $= \frac{1}{T}$ for ideal gas.

The boundary condition equations can be formulated exploiting Equations 21 and 23. For the temperature field, the boundary conditions can be of the first, second, or third kind. Correspondingly, for the pressure field the boundary conditions can be of the first or second kind.

In addition, we have assumed the non-slip velocity and temperature boundary conditions at an interfacial surface of two permeable layers (note Channabasabba 1983; Tong and Subramian 1985).

Consider a space Ω bound by a surface Γ. The average heat flows is at stationary conditions:

$$\text{(i)} \quad \bar{q} = \frac{1}{\Gamma_1} \int^{\Gamma_1} (\vec{q}_1 + h\,\vec{q}_{m1}) \cdot \vec{n}_1 \, d\Gamma = \frac{1}{\Gamma_2} \int^{\Gamma_2} (\vec{q}_2 + h\,\vec{q}_{m2}) \cdot \vec{n}_2 \, d\Gamma \qquad (25)$$

$$\text{(ii)} \quad \bar{q} = \frac{1}{\Gamma_1} \int^{\Gamma_1} (\vec{q}_1 + h\,\vec{q}_{m1}) \cdot \vec{n}_1 \, d\Gamma = \frac{1}{\Gamma_2} \int^{\Gamma_2} \vec{q}_2 \cdot \vec{n}_2 \, d\Gamma \qquad (26)$$

$$\text{(iii)} \quad \bar{q} = \frac{1}{\Gamma_1} \int^{\Gamma_1} \vec{q}_1 \cdot \vec{n}_1 \, d\Gamma = \frac{1}{\Gamma_2} \int^{\Gamma_2} \vec{q}_2 \cdot \vec{n}_2 \, d\Gamma. \qquad (27)$$

Thus, the control surface can be either the "cold" or the "warm" surface, and it can be either permeable or impermeable. The effect of convective flows on the thermal performance of a structure is often expressed with the Nusselt number defined by Equation 28.

$$Nu = \frac{\bar{q}}{\bar{q}_0} = \frac{\int_\Gamma q \, d\Gamma}{\int_\Gamma q_0 d\Gamma}, \qquad (28)$$

where

q_0 denotes the heat flux for pure conduction.

In general, heat fluxes in Equation 28 should be calculated according to convection on the control surface. Thus for the case of a two-dimensional structure the Nusselt number gets the form

$$Nu = \frac{\int_h [\alpha_k(y) \pm c_{p,f}\, q_{m,f}] \, [T_E(y) - T(0,y)] \, dy}{\int_h \alpha_{k,o}(y) \, [T_E(y) - T_0(0,y)] \, dy} \qquad (29)$$

where the quantities with subscript 0 refer to pure conduction; y denotes the coordinate along the control surface; and h denotes the height of the structure.

The convective heat transfer coefficient, α_k, is calculated using correlations for natural / forced convection on a plate or on a room space wall. Signs (+/-) in Equation 29 should be taken to correspond to the viscous flow direction in relation to the direction of convective heat transfer.

Computer Simulation

For analyzing thermal effects of natural / forced convective flows in two-dimensional wall structures, computer code CCC2D has been implemented by Kohonen et al. (1985). The present version solves Equations 24, 21, 23, and 29 in sequence at stationary conditions exploiting the finite difference approach with nonequidistance space differentiation. The wall structure can be multilayered with the following boundary conditions:

pressure field: the 1st or 2nd kind

temperature field: the 1st, 2nd, or 3rd kind.

The moisture transfer by diffusion and convection can also be analyzed. CCC2D is included in our simulation package TRATMO.

Material properties such as thermal conductivity and the viscosity and density of fluid can be functions of temperature. Correspondingly, thermal conductivity and permeability can have

different values in different directions. Convective heat transfer coefficients are calculated from the correlations either for natural or forced convection on a plate / wall.

In order to verify the introduced numerical method, simulations on some laboratory experiments were carried out. The wall structure in the simulation and experiment was 2,2 m high; it had 300-mm-thick glass wool insulation cavity (ρ = 19 kg/m^3, $K_{V,x}$ = 2,1 • 10^{-9} m^2, $K_{V,y}$ = 3,9 • 10^{-9} m^2, $K_{q,y}$ = 0,034 W/m•K); and the temperature difference between the warm and cold air spaces was about 40 ^{o}C. The horizontal boundaries were thermally insulated. In calculations, the heat flux through them were to be zero.

Two different experiments were simulated: absolutely closed cavity and a structure with permeable outer (cold) surface. The wall structure was presented as a fibrous insulating material cavity, closed or open at the outer surface. The heat transfer resistance of the inside surface fiberboard was combined with the inside surface convective heat transfer coefficient. The heat transfer resistance of the thinner outside surface fiberboard was omitted.

It should be noted that to maintain constant temperatures, air had to be circulated with fans on both sides of the structure and thus forced convection appeared on the vertical boundaries. In a numerical solution with boundary conditions of the third kind at vertical surfaces, the convective heat transfer coefficients were calculated assuming pure natural convection, and so the real experimental situation could not be precisely simulated. Therefore, boundary conditions of the first kind were used in the numerical simulations, i.e., the measured temperature distributions on vertical boundaries were given. Figure 4 shows the calculated and measured temperature profiles. The calculated surface temperatures differ from the measured ones as could be expected, since the calculated convective heat transfer coefficients were not expected to be realistic because of the assumption of pure natural convection on vertical surfaces. Figures 5 and 6 give the flow field and heat flux profiles according to calculations.

The convection seems to have been stronger in the experiment than was indicated by the numerical simulation. A reason for the differences may partly be that the heat flux through the horizontal boundaries was not exactly zero, as it was assumed in the numerical solution. It is also possible that in the insulated space, which was assembled with 100-mm-thick mineral fiberboards against smooth horizontal plates, there existed joints and cracks, which contributed to convective flow. In calculations, the effect of these nonideal flows could not be taken into account.

In the case of a structure with open outer surface, the temperature field was solved giving the measured surface temperature values as boundary conditions. The calculated temperature values were in better agreement with the measured than in the case of an enclosure. At corresponding vertical lines, the maximum temperature difference between the measured and calculated is about 2 ^{o}C and the mean temperatures are approximately equal. The shape of the temperature profiles were also approximately the same, though the calculated profiles are at right angles to the horizontal surfaces, which is due to the assumption of an adiabatic surface.

Figure 7 gives a summary of results of the computer simulations, e.g., the dependency of the Nusselt number on the modified Rayleigh number and on the aspect ratio for closed structures and a structure with permeable outer (cold) surface (Kohonen et al. 1985). As we can see in Figure 7, our results are in good agreement with the calculated results for closed enclosure presented by Bankvall (1974).

In Figure 7 it should be noted that in order to have $Ra^* \gg 5$, either the hydraulic conductivity or the mean temperature of insulation should be extremely low as far as ordinary wall structures are concerned.

With Ra^* = 3,4 corresponding to the experimental situation used in verification of the numerical method, the Nusselt number for the open structure is Nu = 1,033. With medium-weight (35 kg/m^3) mineral wool insulating material (Ra^* = 2,2) calculations give Nu = 1,013. Thus the effect of natural convection on the k-value of a wall structure with medium-weight mineral wool insulating material is, from the practical point of view, nearly insignificant.

Correspondingly, when the outer vertical 50-mm layer of lightweight mineral wool insulating material space was replaced with a glass wool wind shield, with the specific permeability one-tenth that of the insulating material, and with thermal conductivity K_q = 0,045 W/m•K, calculations give Nu = 1,044. Thus, in this case the glass wool wind shield cuts down the mean heat flow increase caused by natural convection by only about one-half. When the specific permeability of wind shield was one-fifth of the value of the previous cases, Nusselt's number of 1,013 was obtained.

With a 50-mm-thick wind shield with specific permeability $K_{v,x} = 6,4 \cdot 10^{-11}$ m^2 or less natural convection has an insignificant effect on the k-value of the structure. With a 12-mm-thick wind shield with $K_{v,x} = 10^{-12}$ m^2 or less, the structure corresponds to an enclosure in a thermal sense.

If a thin, horizontal obstruction (plate), having the same horizontal thermal conductivity as the insulating material, is placed at the height of 1,16 m in the open wall structure, the calculation gives Nu = 1,051. So the mean heat flux through the wall is decreased, though in the case of a single cavity with approximately the same aspect ratio (3,67), it is increased, compared with the case h/d = 7,33. This is caused by internal heat flow through the obstruction plate from the warmer part to the colder part of the structure.

As it can be seen in Figure 8, the thermal performance of the structure is like that of two separate wall with the aspect ratio 3,67, if the heat flow between the two cavities is restricted.

The former calculations represent natural convection in a vertical wall structure. If the permeable parts of different wall structures are coupled, the flow field of one structure will have an influence on the flow fields of the others. Therefore, the thermal performance of the whole building envelope differs considerably from what would occur if each structure behaved separately.

As an example for joined wall structures, a vertical wall consisting of a 50-mm glass wool wind shield and 250-mm lightweight mineral wool insulating material was considered. The inside height of the wall was 2,5 m and the inside length of the horizontal part was 1,0 m. The inside and outside air temperatures were 293 and 253 K, respectively. The structure was simplified so that the crossbars were omitted and only the porous parts of the structure were presented. The outer surfaces of the wind shield and the horizontal layer were permeable and the other surfaces were impermeable.

In the case of natural convection, the Nu-values calculated for the inside vertical and horizontal surfaces were 1,11, and 0,80, respectively. The decrease of the Nu-value of the horizontal part was caused by a rising flow that warmed up the horizontal parts of the insulating material near the corner. The flow field and heat flux profiles are shown in Figure 9.

Laboratory Experiments

Laboratory experiments were carried out in order to

- get a better understanding of extra heat transfer due to natural convection in full-scale wall structures with thermal insulation assembled with standard-size fiber insulation boards and mats,
- find out differences between an ideal and a real insulation, i.e., between calculations and experiments.

Test walls with four separate insulation spaces were exposed to warm and cold room spaces kept practically at constant temperatures (Figure 10). The height, breadth, and thickness of each insulation space were 2,2 m, 0,55 m, and 0,3 m, respectively. Air leakages between the test insulation and environment were prevented with an airtight envelope and sealings in joints, except in the case of open cold surface. The permeability and thickness of mineral fiber insulation with / without (vertical or horizontal thermally well-conductive convection obstructions), permeance of wind-shield board, and the cold room air temperature were varied in experiments. The air temperature in the warm side was constant (about 22 ^{o}C) in all experiments.

Temperature profiles were measured with thermocouples located at different levels and depths in the middle section of the test structures. Correspondingly, heat flux profiles were measured on the warm impermeable surface with heat flux meters. Measurements were carried out under steady-state conditions. Altogether 22 different structures were measured, each at three different mean temperatures (changing the temperature of the cold room space between +6 ^{o}C - -20 ^{o}C).

The experimental Nusselt numbers (Nu^*) were determined using the following approach giving a lower approximation. The average heat flux with the lowest temperature difference for each structure was assumed to represent the pure conductive heat flux giving $Nu^* = 1$ (i.e., the reference value). The temperature dependence of the thermal conductivities of insulation and

wind shield materials was taken into account by a correction factor. The experimental Nusselt numbers are determined by Equation 30 :

$$Nu^* = \bar{q} \Big/ \left(\frac{\overline{q_o}}{\overline{\Delta T_o}} + \Delta k \right) \overline{\Delta T} , \qquad (30)$$

where

$\bar{q}$ is the mean heat flux in the experiment, W/m^2

$\overline{q_o}$ the mean heat flux in the "convection-free" reference experiment, W/m^2

Δk the calculated correction factor of "convection-free" thermal transmittance due to the temperature dependence of thermal conductivities, $W/m^2 \cdot K$

$\overline{\Delta T}$ the mean temperature difference between the warm surface of insulation and the cold air space, K

$\overline{\Delta T_o}$ corresponding mean temperature difference in the "convection-free" reference experiment, K

Table 1 gives a summary of measurements. In general, the dependence of the experimental Nusselt numbers on the effective parameters was logical only case by case. Therefore, simulation had to be applied. Based on the results of experimental studies, some practical aspects and conclusions can, however, be given.

In the present work, test insulations were nearly full scale (of small house size) and made of one or several insulation layers. In spite of efforts to avoid faults in insulation and tightening, many insulations behaved unforeseeably with regard to natural convective heat transfer. Difficulties in practical are obviously similar, e.g., insulation work can hardly be as good as in laboratory conditions.

Experimental results show the equal convection effect as, or stronger than, what could be expected according to the computer simulation. The test insulation structures seem to be more or less successful approximations to ideal ones. Some experimental results, however, support the calculated results, which can be considered as lower approximations.

The only results giving $Nu^* \approx 1$ were measured for the insulation structures with one 0,1-m-thick insulation layer between two airtight impermeable vertical surfaces. With two or three layers of insulation material, the Nu^*-numbers were always higher than expected. Obviously, increasing the number of boundary layers between insulation and covering surfaces caused stronger convection than expected. The horizontal convection obstruction did not bring any advantage.

The thermal resistance of insulated wall structure decreases owing to natural convection and increases owing to the temperature dependence of thermal conductivities, if the temperature is kept constant inside and lowered outside the structure. The effects compensate each other. In the experiments both effects were approximately as strong, e.g., the thermal resistances of the insulation structures in experiments were approximately constant in the temperature region used in experiments, for $Nu^* = 1{,}03$ and $Nu^* = 1{,}09$ at the mean temperatures 283 K, respectively.

WARMING UP OF LEAKAGE AIR IN CRACKS

The actual heating load of building often differs from the designed load. One reason for this is the uncontrolled (infiltrations) ventilation through a building envelope. Hydraulic properties of different leakage routes have been studied widely, and leakage flow rates can nowadays be predicted rather well. The warming up of leakage air has not, however, been studied, and therefore it has been difficult to predict the real heating load due to leakage. In practice, the heating load of leakage ventilation has been calculated assuming that the air flows in at the outside temperature.

Leakage air is warmed by exploiting the conductive heat losses of a structure. Therefore both conductive and convective flows affect the temperature field of the structure. Applying Equation 3 the heat balance of the flowing component can be written in the form

$$\frac{\partial}{\partial t}\langle\rho_f h_f\rangle = -\nabla\cdot\langle\vec{q}_f\rangle - \nabla\cdot\langle h_f\vec{q}_{m,f}\rangle - \frac{1}{V}\int_{\partial V_{fs}} \vec{q}_f\cdot\vec{n}_{fs}\, dA \qquad (31)$$

Correspondingly, for the stagnant component, s

$$\frac{\partial}{\partial t}\langle\rho_s h_s\rangle = -\nabla\cdot\langle\vec{q}_s\rangle - \frac{1}{V}\int_{\partial V_{sf}} \vec{q}_s\cdot\vec{n}_{sf}\, dA. \qquad (32)$$

The heat transfer between components s and f can be given by Equation 33

$$\int_{\partial V_{sf}} \vec{q}_s\cdot\vec{n}_{sf}\, dA = \int_{\partial V_{sf}} \alpha_{sf}\,(T_s - T_f)\cdot\vec{n}_{sf}\, dA\ , \qquad (33)$$

Assuming stationary conditions, bulk flow, and constant transport properties, we get for the temperature of the flow component a certain distance, s , from the inlet of a crack :

$$T_f(s) = \left(T_f(o) + \int_o^s g(s)e^{\varphi(s)}ds\right)e^{-\varphi(s)}\ , \qquad (34)$$

where

$$\varphi(s) = \int_o^s \frac{\alpha_{sf}(s)P\,ds}{q_{m,f}c_{p,f}}$$

$$g(s) = \frac{\alpha_{sf}(s)P(s)}{q_{m,f}c_{p,f}}\,T_{s,sf}(s).$$

In Equation 34 $T_f(o)$ and P denote the inlet temperature of the flow component and the circle of the crack, respectively.

Numerical integration can be applied in Equation 34, if the surface temperature of crack network is known. The surface temperature depends on the wall construction and on the flow rate through the thermal coupling, Equation 33. Consequently, Equations 31 and 33 should be solved simultaneously, e.g., $T_f(s)$ is given as a boundary condition in solving the temperature field of a structure, Equation 32, omitting the surface integral on the right-hand side.

The method described above has been used to solve the heating of leakage air in some typical, idealized cracks (Kohonen et al. 1985). Also the effect of leakage air on the thermal behavior of structures has been considered. Let us first consider the heating of leakage air in a crack between a timber frame wall and window frame and in a crack between a timber frame wall and foundation, Figure 11 . The leakage flow rates are in both cases q_V = 0,2 dm^3/sm, 0,7 dm^3/sm, and 2,0 dm^3/sm. The convective heat transfer coefficients at the inner and outer surfaces of the structure are 8 $W/m^2\cdot K$ and 13 $W/m^2\cdot K$ and the inside and outside temperatures are constant 20 ^oC and -10 ^oC, respectively.

Figure 12 shows the heating of the leakage air as a function of the length of leakage route for different flow rates. It can be seen that the heating is most significant with low leakage flow rates.

Figure 13 gives the corresponding heat flux profiles.

The heating of leakage air does not directly correspond to the heating load of a building, because leakage flows also affect the conductive heat flow field of the structures.

In steady-state considerations, the heat balance surface can be set at the outer surface of the envelope. Then the heat flux at the outer surface represents the conductive (transmission)

heat losses and the thermal effect of infiltrating air can be evaluated by changes. For the crack between window frame and wood wall (Figure 11) Nusselt's numbers defined as the ratio between transmission heat fluxes at the outer surface of a structure in the cases of pure and infiltration affected conduction are $Nu_{0,2} = 0,77$, $Nu_{0,7} = 0,64$, and $Nu_{2,0} = 0,60$. Correspondingly, for the crack between wall structure and foundation, Nusselt's numbers are $Nu_{0,2} = 0,83$, $Nu_{0,7} = 0,68$, and $Nu_{2,0} = 0,60$. This result show that the heating load of transmission and infiltration is usually overestimated by tens of percents.

Let us finally consider the significance of the warming up of the leakage air with an example from practice. Our example building is provided with an exhaust ventilating system.

The heating load of the building was also determined by calculation and measurements. The thermal transmittance representing the transmission heat losses was 820 W/K. The capacity flow rate of the exhaust air was (according to measurements) 1370 W/K. The mean underpressure of the inside air was 12 Pa. Thus the measured airflow rate represents the total ventilation. The mean inside temperature was 23 °C. Figure 14 shows measured and calculated heating loads of the building as a function out the outdoor temperature. We can find out that Nu = 0,8 gives the measured heating load.

Our calculations (Kohonen et al. 1985) show that the warming up of leakage air is rather efficient on typical leakage routes. With allowable leakage flow rates in relation to thermal comfort (0,5 - 0,7 dm^3/sm) the heating is 25 - 60 % of the outside and inside temperature difference corresponding to Nusselt's numbers 0,9 - 0,7. Based on this fact, we suggest the heating load of infiltration / exfiltration and transmission to be calculated according to Equation 35

$$\phi = \left(-q_{m,i}T_o + \sum_e q_{m,e}T_e + (q_{m,i}-q_{m,e})\,T\right) c_p + \\ + \left(\sum_i Nu_i \bar{k}_i A_i + \sum_e Nu_e \bar{k}_e A_e + \sum_{cc} Nu_{cc} \bar{k}_{cc} A_{cc} + \sum_c \bar{k}_c A_c\right)\left(T - T_o\right) \qquad (35)$$

where subscripts i, e, cc, c, o denote infiltration, exfiltration, convection and conduction, pure conduction, and outdoor, respectively. T is the indoor temperature and $\bar{k}$ the overall average thermal transmittance (k-value) of a structure.

ASPECTS OF THE INFLUENCE OF MOISTURE

When considering the thermal performance of a wall structure, we should note that circumstances of pure conduction do not occur very often. For example, in a vertical structure with well-permeable materials, natural convection occurs although the average heat flux may correspond to pure conduction. Fruther, in thin high-porosity insulating materials, radiative heat transfer may cause non-Fourier-type behavior. Moisture affects the thermal performance of a wall structure in three ways: stagnant moisture (water and ice) has much higher thermal conductivity than dry/humid air; moisture flow in liquid / vapor phases means convective heat transfer; interstitial phase changes also cause extra heat transfer compared with pure conduction.

In a structure exposed to a natural climate, the rate of latent heat transfer owing to interstitial phase changes depends naturally on the time-dependent indoor and outdoor hygrothermal conditions, e.g., on the rate and modes of moisture transfer. Therefore, to analyze influence of moisture on the thermal performance of a wall structure, we must have the simultaneous knowledge of temperature and moisture fields, which in most cases means the exploitation of computer simulation to solve Equations 12 and 14 with proper boundary conditions.

Under steady-state conditions, moisture is accumulated in the colder parts (surfaces) of a structure while the rest of the body is relatively dry. Therefore, we may get values for thermal conductivities / thermal tansmittances nearly corresponding to those with dry materials, although the average moisture contents were relatively high. This is obvious, if we note that the thermal resistance of a multilayer structure (in one-dimensional case) is

$$M = \sum_i M_i = \sum_i (\Delta x_i/\lambda_a) = \sum_i \Delta T_i / q\,, \qquad (36)$$

where q and λ_a denote the steady-state heat flux and apparent (overall) thermal conductivity, respectively. According to Equation 14 the total heat flux is

$$\vec{q}_T = -\underline{K}_q \cdot \nabla T + \ell_{\alpha\beta}(\vec{q}_{m,\alpha} + \vec{q}_{D,\alpha}) + \sum_\alpha h_\alpha \vec{q}_{m,\alpha} \quad . \tag{37}$$

Omitting convective heat flux and assuming saturation conditions we get

$$\vec{q}_{T,D} = -\left[\underline{K}_q + \frac{\underline{K}_D D_{14} M_1^2}{R^2 T^3} \ell_{12}^2 p_{1,0}^{(14)}(T) \right] \cdot \nabla T \quad . \tag{38}$$

We should note that, in practice, we do not very often have conditions where Equation 38 is valid. In experiments, total heat fluxes corresponding to Equation 38 are obtained when water is sprayed on the hot surface of a guarded hot plate apparatus (Langlais 1983). Conditions corresponding to Equation 38 are also obtained when there is a closed system where the total moisture flux is zero owing to the so-called heat pipe effect.

In Figure 15 three different curves for the thermal conductivity of moist fibrous insulant are given. The first curve (Jespersen 1953) is obviously measured under conditions where the heat pipe effect is present. In this case, Equation 38 describes the latent heat transfer. The second curve (Langlais 1983) is measured with a douple-guarded hot plate apparatus. In this measuring procedure, moisture is redistributed (moisture accumulates at the cold surface/parts of insulant), while the rest of the test body is relatively dry. This explains the relatively slight dependency of the thermal conductivity on moisture content. We have obtained corresponding values from steady-state laboratory experiments with wall structures of real life (Kohonen 1986).

Either of the λ-curves does not represent the Fourier thermal conductivity of moist fibrous insulant, because moisture is not stagnant nor uniformly distributed. The third curves are obtained with a transient method (Katayama 1973; Kohonen 1984). As seen in Figure 15, also this method is very sensitive to the condition applied in experiments. With extrapolation ($dT/dx \rightarrow 0$), the Fourier thermal conductivity of moist glas fiber insulant could be determined.

In order to evaluate the practical effect of moisture and moisture transfer on the thermal performance of a wall structure exposed to a natural climate, we should consider the influence of stagnant moisture on the Fourier thermal conductivity and heat transfer owing to interstitial phase changes. The modes of moisture transfer and the moisture content of materials in a structure depend naturally on the boundary conditions. Consequently, the apparent k-value / thermal conductivity of a structure / insulation layer, where also moisture transfer occurs, should be based on the time averaged heat flux and temperature difference:

$$\bar{k}_a = \frac{\int_t \left(\int_\Gamma q \, d\Gamma \right) dt}{\Gamma \int_t \Delta T \, dt} \quad , \tag{39}$$

where q and Γ denote the total heat flux (Equation 37) and the control surface, respectively. Figure 16 shows temperature and heat flux profiles in a flat roof construction exposed to a natural climate in Southern Finland. The apparent k-value of the insulation layer for the one week's period is $k_a = 0{,}25$ W/m^{2}K corresponding to $\lambda_a = 0{,}056$ W/m·K. The moisture content distribution was rather uniform giving $u = 4{,}5$ %-by weight on an average.

DISCUSSION

A physical and mathematical model for heat and mass transfer in porous media has been introduced based on the volume-averaging approach. The model equations take into account diffusive and convective heat and mass transfer as well as interstitial phase changes. The derivation of the balance equations has been given here to show how the coupling between heat and mass (convection and diffusion) transfer is formed. Understanding of coupling is especially important in consideration of heat transfer in moist porous materials in order to be sure you are studying the phenomena you think your are studying.

The continuity, momentum, and energy equations given in this paper have been used in the simulation package TRATMO developed at our institute. The same approach has been used in the development of methods for the determination of heat and moisture transport properties of building materials. The simulation package includes the computer programs, with which the results of the present paper were calculated. Program CCC2D has further been developed so that also convective vapor transfer can be taken into account.

The values for thermal conductivity of moist fibrous insulants are preliminary and do not necessarily represent the Fourier thermal conductivity. Research work in this field will be continued. Radiation heat transfer in porous media, especially in building materials with low density, is often dominant. In this paper radiation and conduction are coupled, i.e., the Fourier thermal conductivity includes the both heat transfer modes. With the material densities and temperature circumstances discussed in this paper, this approach (as the first approximation) seems to be rather reasonable.

It is wellknown from literature at which conditions internal convection flows in a closed filled cavity cause extra heat transfer compared with pure conduction. Building wall structures are, however, more or less leaky and permeable, and therefore those results are not valid. The thermal effects of internal convection flows in wall structures with fibrous insulation given in the present paper are obtained with computer simulation. They show very slight increase in the average heat flux owing to convection, even in a superinsulated wall structure. Laboratory experiments show, however, significantly higher values than calculations, and it is obvious that in practice convection effects on the thermal performance are much higher than what calculations and laboratory experiments show. Furthermore, the building envelope forms a flow system, whose thermal behavior differs from that of an individual wall section.

Hydraulic properties of leakage routes have been studied widely, and nowadays leakage flow rates can be predicted rather well. Heating of leakage air is a new aspect in room air heat balance calculation. In heat balance calculation we should note where the control surface is. In steady-state considerations it is reasonable to consider the outer surface as the control surface. Thus the transmission heat flow is less (higher) in the case of infiltration (exfiltration) flow and the inlet (outlet) temperature of infiltration (exfiltration) air is equal to (less than) the outdoor (indoor) air temperature.

In our further studies on thermal effects of airflows, a counterflow wall structure (dynamic insulation) integrated with the exploitation of solar energy as well as warming up of infiltration air and internal / penetrating convection flows will be analysed more thoroughly using calculation and experiments.

CONCLUSION

Influences of airflows and moisture on the thermal performance of wall structures have been discussed. Two different flow systems were considered: natural / forced convection in two-dimensional building structures and warming up of infiltration air in cracks. Some aspects of the influences of moisture was also introduced.

In a closed, ideally filled vertical wall structure, internal convection has only a slight influence on the average heat flow. Even for a superinsulated (300 mm) wall structure having the Rayleigh number 5,2 and the aspect ratio 7,33 the Nusselt number is 1,006. This does not, however, mean that convection is absent but that the average heat flow corresponds to pure conduction heat flow. The Nusselt number for the same wall structure is 1,08 if the cold surface is permeable. A wall structure can be considered as an enclosure if the permeability of the wind shield is less than 10^{-12} m^2.

Even if internal convective flows had only a slight influence on the average heat flow of a wall structure, they have strong influences on the temperature and heat flux profiles, from which two practical aspects arise. First, it must be somewhat difficult and inaccurate to determine the k-value of a wall structure using heat flux meters owing to nonuniform heat fluxes. Secondly, internal condensation may be more probable than in the convectionless case owing to the cooling effect of convection flows.

Thermal effects of internal convective flows can be reduced with horizontal convection obstructions, which should not be good thermal insulators in order to ensure heat transfer over obstruction from the warm top to the cold bottom of sequent cavities.

Experimental results show the same convection effect as, or stronger than, what could be expected according to the computer simulation. The test insulation structures seem to be more or less successful approximations to ideal ones. Some experimental results, however, support the calculated results. The only results giving the experimental Nusselt number $Nu^* \approx 1$ were measured for the insulation structures with on 0,1-m-thick insulation layer between two airtight vertical impermeable surfaces. With two or three layers of insulation material, the Nu^*-numbers were always higher than expected. Obviously, increasing the number of boundary layers between insulation and covering surfaces caused stronger convection than expected. The horizontal convection obstruction did not bring any advantage in experiments.

The actual heating load of a building is different from the designed load. A reason for this may be uncontrolled infiltration of outdoor air through the exterior building envelope. The heating of infiltrating leakage air exploits the transmission heat loss of the wall structure. For allowable leakage rates (0,5 - 0,7 dm^3/sm), in relation to thermal comfort, the rise in temperature is between 25 - 60 % of the inside / outside temperature difference. The actual value depends on the leakage mass flow rate and the length of the leakage route, as well as on the thermal properteis of the wall structure around the crack. Correspondingly, Nusselt numbers describing the relative reduction of transmission heat flow at the outer surface of the structure are 0,9 - 0,7.

It is suggested that in practical calculations, when the heat balance control surface is put on the outer surface of exterior building envelope, the value of the transmission heat flow without infiltration should be multiplied by the Nusselt number in order to have correct (valid with infiltration) transmission heat flow, e.g., in order not to overestimate the heat load of transmission and infiltration. Correspondingly, the k-value of a structure, where also moisture transfer occurs, should be based on the time averaged heat flux and temperature difference over the structure.

NOMENCLATURE

B = hydraulic conductivity, $1/m^2$

C''' = volumetric heat capacity of porous composition material, J/m^3K

$c_{p,i}$ = isobaric specific heat capacity of constituent i, = $(\partial h_i/\partial T)_p$, J/kgK

Da = Darcy number, = K_v/d^2

D_{14} = diffusion coefficient for water vapor in humid air, m^2/s

d = width of the porous layer, m

$\vec{f}_i$ = external body force of constituent i, N/kg

g = gravity force, = 9,81 m^2/s

h_i = enthalpy of constituent i, J/kg

$\underline{K}_D$ = diffusion obstruction factor

$\underline{K}_{q,i}$ = thermal conductivity of constituent i, $W/m \cdot K$

$\underline{K}_{v,i}$ = permeability for constituent i, m^2

L = characteristic length of the porous media, m

ℓ_{ij} = latent heat of the phase change ij, J/kg

M_i = molecular mass of constituent i, kg/mol

Nu = Nusselt number, defined in text

Nu^* = experimental Nusselt number, defined in test

$\vec{n}_{ij}$ = unit normal vector of the interfacial surface ∂V_{ij}

Pe^* = modified Peclet number, = $\frac{vL}{D_{14}}$

p_i = pressure of constituent i, N/m^2

$p_{1,0}^{(14)}$ = saturation water vapor pressure of free water, N/m^2

$p_1^{(14)}$ = saturation water vapor pressure of bond water, N/m^2

$\vec{q}_D$ = diffusion mass flux, $kg/m^2 \cdot s$

$\vec{q}_{eff}$ = efflux

$\vec{q}_i$ = heat flux in constituent i, W/m^2

$\vec{q}_m$ = convective mass flux, $kg/m^2 \cdot s$

$\dot{q}_{m,ij}$ = rate of the interstitial phase change from phase j to i, $kg/m^3 \cdot s$

$\vec{q}_T$ = total heat flux, W/m^2

$\vec{q}_V$ = viscous flux, $kg/m^2 \cdot s$

R = universal gas constant, = 8314 J/kmol K

Ra^* = modified Rayleigh number, $= g\beta \left(\frac{\rho c_p}{\nu}\right)_f \Delta T d \; \frac{4 K_{v,x} K_{v,y}}{\left[(K_{q,y} K_{v,x})^{\frac{1}{2}} + (K_{q,x} K_{v,y})^{\frac{1}{2}}\right]^2}$

T = temperature, K or ^oC

t = time, s

$\underline{t}_i$ = stress tensor of constituent i, N/m^2

u = moisture content

V_i = subvolume of constituent i, m^3

∂V_i = boundary surface of subvolume V_i, m^2

∂V_{ij} = interfacial surface of constituents i and j, m^2

$\vec{v}_i$ = velocity of constituent i, m/s

$\vec{w}_{ij}$ = velocity of the interfacial surface ∂V_{ij}, m/s

β = thermal expansion coefficient, 1/K

Γ = control surface, m^2

η_i = viscosity of constituent i, kg/m s

λ = thermal conductivity of isotropic material, $W/m \cdot K$

λ_a = apparent thermal conductivity, $W/m \cdot K$

ν_i = kinematic viscosity of constituent i, m^2/s

$\langle \rho_i \rangle$ = partial density of constituent i, kg/m^3

$\langle \rho_i \rangle^{(i)}$ = density of constituent i, kg/m^3

$\underline{\tau}_i$ = shear stress tensor of constituent i, N/m^2

VOLUME AVERAGED QUANTITIES:

$$\langle \Psi_i \rangle^{(i)} = \frac{1}{V_i} \int_{V_i} \Psi_i \, dV$$

$$\langle \Psi_i \rangle^{(i)} = \frac{1}{V_j} \int_{V_i} \Psi_i \, dV$$

$$\langle \Psi_i \rangle = \frac{1}{V} \int_{V_i} \Psi_i \, dV$$

SUB- AND SUPERSCRIPTS:

inert solid	0
water vapor	1
surface adsorbence and capillary condensate	2
capillary condensate	3
inert gas (dry air)	4
humid air	14
gaseous and liquid moisture	12
fluid	f
solid	s
environment	E

REFERENCES

LUIKOV, A.V. 1961. Heat and mass transfer in capillary-porous bodies. Oxford: Pergamon Press.

LAMPINEN, M. 1979. Mechanics and thermodynamics of drying. Acta Polytechnica Scandinavica, Mechanical Engineering Series, Me 77.

KIESSL, K. 1983. "Kapillarer und dampfförmiger Feuchtetransport in mehrsichtigen Bauteilen". Ph.D. Dissertation. University of Essen.

DINULESCHU, H. A. 1980. "An application of irreversible thermodynamics to the problem of heat moisture migration in soil". Wärme- und Stoffübertragung, Vol. 13, No 1/2, pp. 11-25.

KOHONEN, R. 1984. "A method to analyze the transient hygrothermal behaviour of building materials and components". Technical Research Centre of Finland, Publications, No 21.

SLATTERY, J. C. 1972. Momentum, energy and mass transfer in continue. New York: Mc Graw-Hill, Inc.

GRAY, W. G. 1975. "A derivation of the equations for multi-phase transport". Chem. Eng. Sci., Vol. 30, No 2, pp. 229 - 233.

BEAR, J. 1972. Dynamics of fluids in porous media. New York; Elsevier.

KOHONEN, R. and MÄÄTTÄ, J. 1981. "Transient analysis of the thermal and moisture physical behaviour of building constructions". Technical Research Centre of Finland, Research Reports, No 168.

CHANNABASABBA, M. N. 1983. "Convective heat transfer in a parallel plate channel with porous lining". Wärme- und Stoffübertragung, Vol. 17, No 4, pp. 211 - 216.

TONG, T. W. and SUBRAMANIAN, E. 1985. "A boundary-layer analysis for natural convection in vertical porous enclosures - use of the Brinkman - extended Darcy model". Int. J. Heat Mass Transfer, Vol. 28, No 3, pp. 563-571.

KOHONEN, R.; KOKKO, E.; OJANEN, T.; and VIRTANEN, M. 1985. "Thermal effects of air flows in building structures". Technical Research Centre of Finland, Research Reports, No 367.

BANKVALL, C. G. 1974. "Natural convection in vertical permeable spaces". Wärme- und Stoffübertragung, Vol. 7. No 1, pp. 22 - 30.

LANGLAIS, C.; HYRIEN, M.; and KLARSFELD, S. 1983. "Influence of moisture on heat transfer through fibrous-insulating materials". Thermal Insulation, Materials, and Systems for Energy Conversation in the 80's. ASTM STP 789, F. A. Govan, D.M. Greason and J.D. McAllister, Eds., American Society for Testing and Materials, 1983, pp. 563 - 581.

KATAYAMA, K.; HATTARI, M.; KASAHARA, K.; KIMURA, I.; and OKADA, M. 1974. "Thermal properties of wet porous material near freezing point. A transient simultaneous method". ASHRAE-Journal, April 1974, pp. 56 - 61.

JESPERSEN, H. B. 1953. Journal of the Institute of Heating and Ventilation Engineering, Vol. 21, No 216, Aug. 1953, pp. 157 - 174.

KOHONEN, R. 1986. "Influence of moisture transfer on the thermal performance of structures with fibrous thermal insulant". To be published in 1986 in Technical Research Centre of Finland, Research Reports.

TABLE 1

Temperature Conditions and the Experimental Nu* Values of Test Insulations

Thermal insulation Material/layers	h/d	Wind shield	Mean temperature of insulation (T_m), mean temperature difference between the warm surface of insulations and cold air space (ΔT), experimental Nusselt's number (Nu*)	
			T_m (K)/$\overline{\Delta T}$ (K)/Nu*	T_m (K)/$\overline{\Delta T}$ (K)/Nu*
glas fibre mat 17 kg/m^3				
1 x 100 mm	22	open cold surface	278/26.3/1.03	272/37.4/1.05
1 x 100 mm	22	plywood 6 mm	279/25.5/1.00	272/37.0/1.00
2 x 100 mm	11	open cold surface	279/26.6/1.04	274/36.2/1.08
2 x 100 mm	11	plywood 6 mm	281/24.6/1.02	274/36.4/1.06
2 x 100 mm	11	diabase fibre board 90 kg/m^3, 30 mm	282/26.0/1.02	277/36.2/1.06
2 x 100 mm vertical convection obstruction at x = 100 mm	11	plywood 6 mm	278/27.0/1.00	273/36.1/1.00
3 x 100 mm	7.3	open cold surface	277/29.2/1.06	271/34.6/1.16
3 x 100 mm	7.3	plywood 6 mm	281/25.1/1.09	275/36.9/1.21
glas fibre mat 19 kg/m^3				
2 x 100 mm	11	open cold surface	279/26.9/1.01	274/36.9/1.04
2 x 100 mm	11	plywood 6 mm	281/26.1/1.01	275/36.9/1.02
2 x 100 mm horizontal obstruction at h = 1.1 m	11	plywood 6 mm	277/26.5/1.02	272/33.6/1.07
2 x 50 + 100 mm vertical convection obstruction at x = 50 mm	11	plywood 6 mm	279/27.7/1.03	272/41.6/1.06
3 x 100 mm	7.3	open cold surface	281/25.8/1.02	275/38.1/1.09
3 x 100 mm	7.3	plywood 6 mm	278/27.5/1.01	273/39.7/1.04
Diabase fibre board 35 kg/m^3 (1320 x 565 mm)				
1 x 100 mm	22	open cold surface	278/26.7/1.04	272/37.8/1.13
1 x 100 mm	22	plywood 6 mm	278/26.5/1.00	272/38.6/1.00
2 x 100 mm	11	open cold surface	280/26.6/1.03	274/36.2/1.09
2 x 100 mm	11	bituminous wood fibre board	281/25.5/1.01	275/37.4/1.05
2 x 100 mm	11	diabase fibre board 90 kg/m^3, 30 mm	282/26.4/1.03	277/37.0/1.07
3 x 100 mm, 1 - 3 mm cracks in horizontal joints of two layers	7.3	open cold surface	278/29.5/1.11	274/35.1/1.19
3 x 100 mm, with full high boards	7.3	open cold surface	278/28.3/1.03	272/37.6/1.08
3 x 100 mm	7.3	plywood 6 mm	282/25.0/1.04	275/37.3/1.09

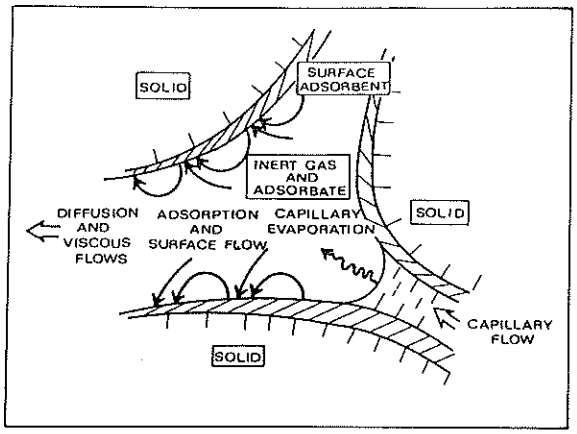

Figure 1. Physical model for moisture transfer in porous media

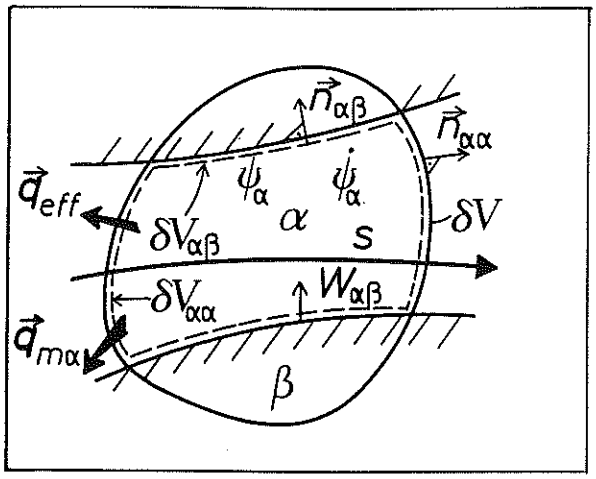

Figure 2. Binary system using concepts from Equation 3

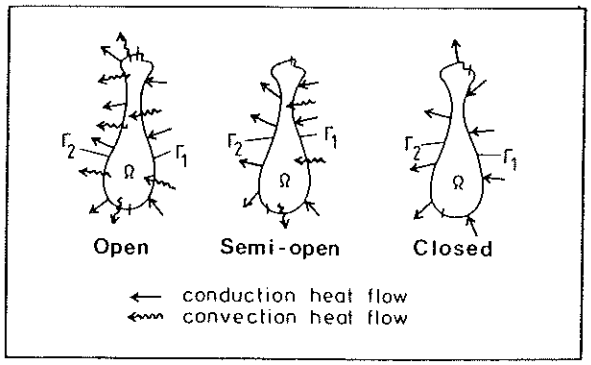

Figure 3. Physical model for Equations 25-27

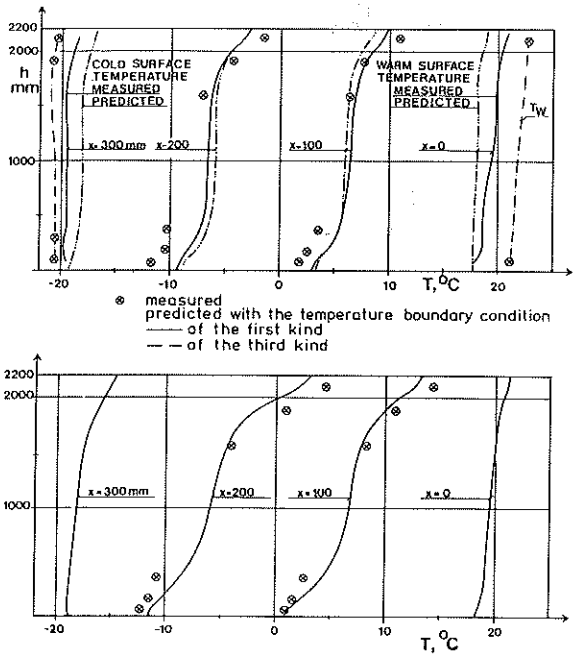

Figure 4. Experimental and calculated temperature profiles in closed (upper) and open (lower) filled cavity

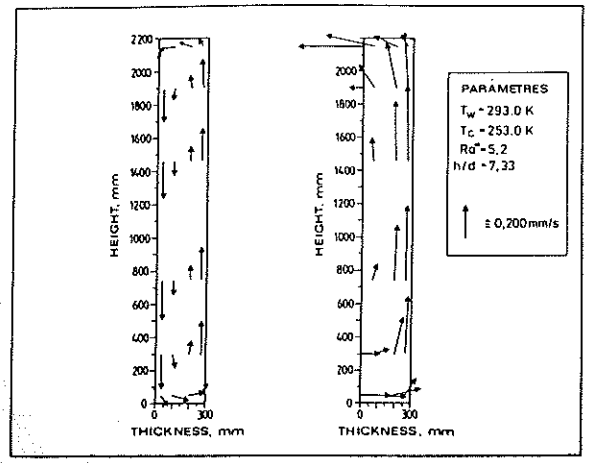

Figure 5. Calculated flow fields for closed and open structure (Ra^* = 5, 2; h/d = 7, 33)

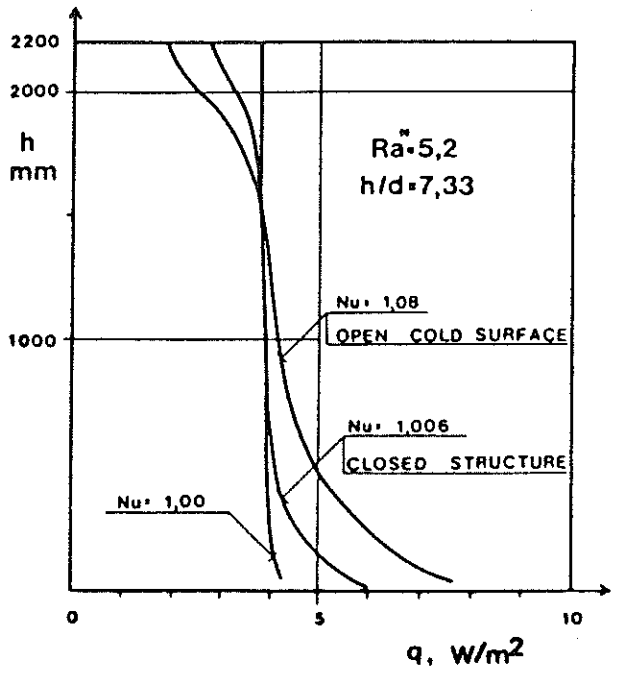

Figure 6. Calculated heat flux profiles corresponding to Figure 5

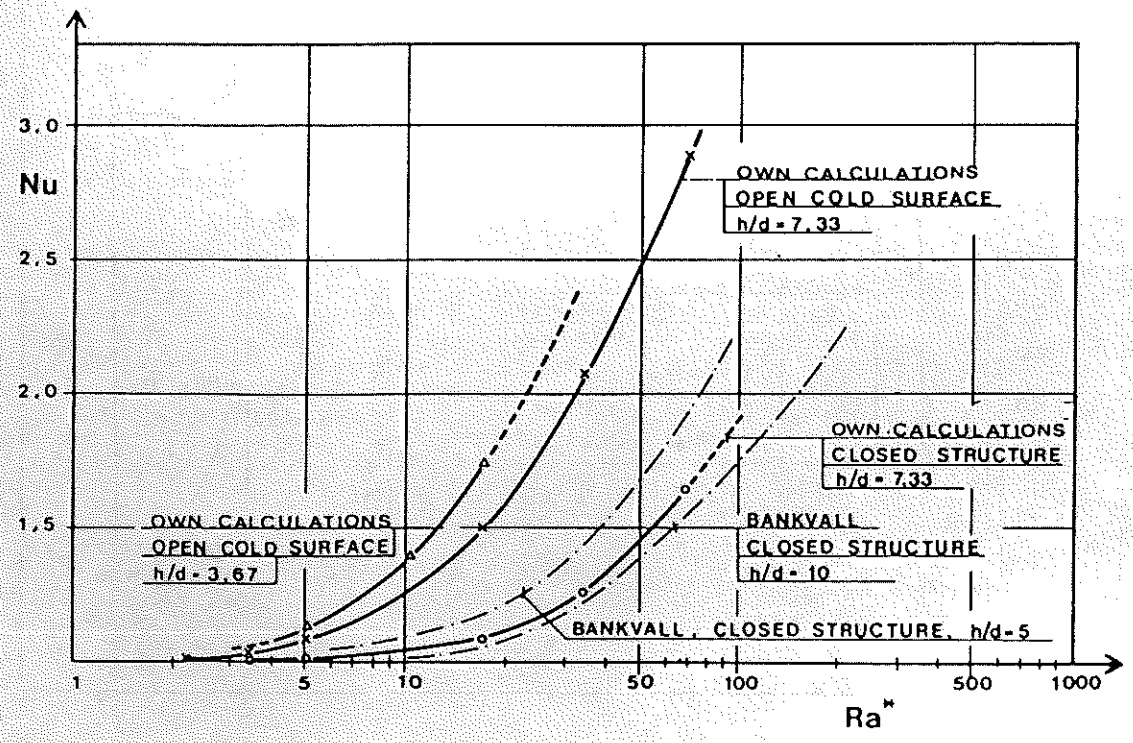

Figure 7. Nusselt number as function of modified Rayleigh number (Kohonen et al. 1985)

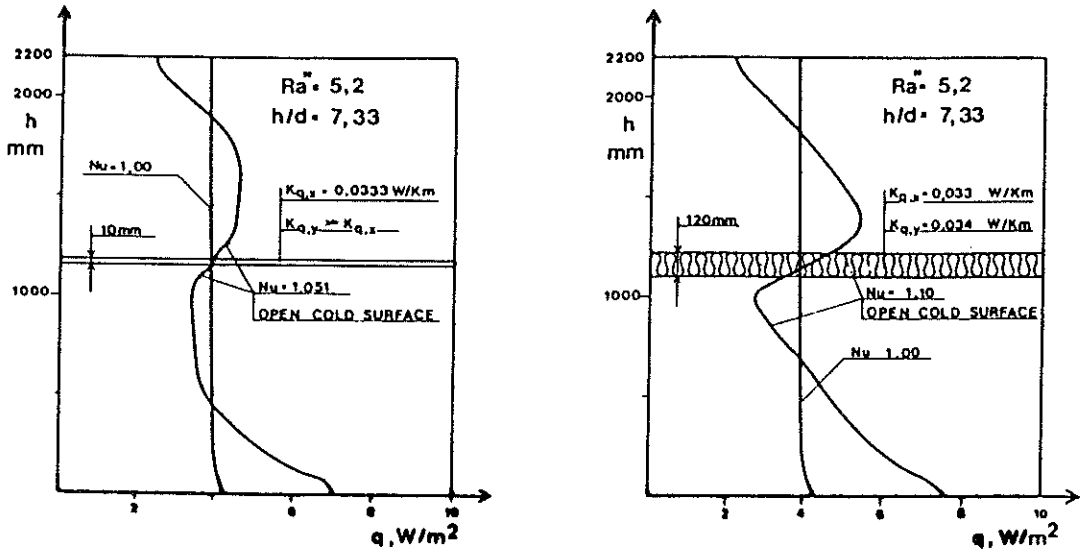

Figure 8. Calculated heat flux profiles for wall structures with permeable cold surface and with well- or nonconductive horizontal convection obstruction

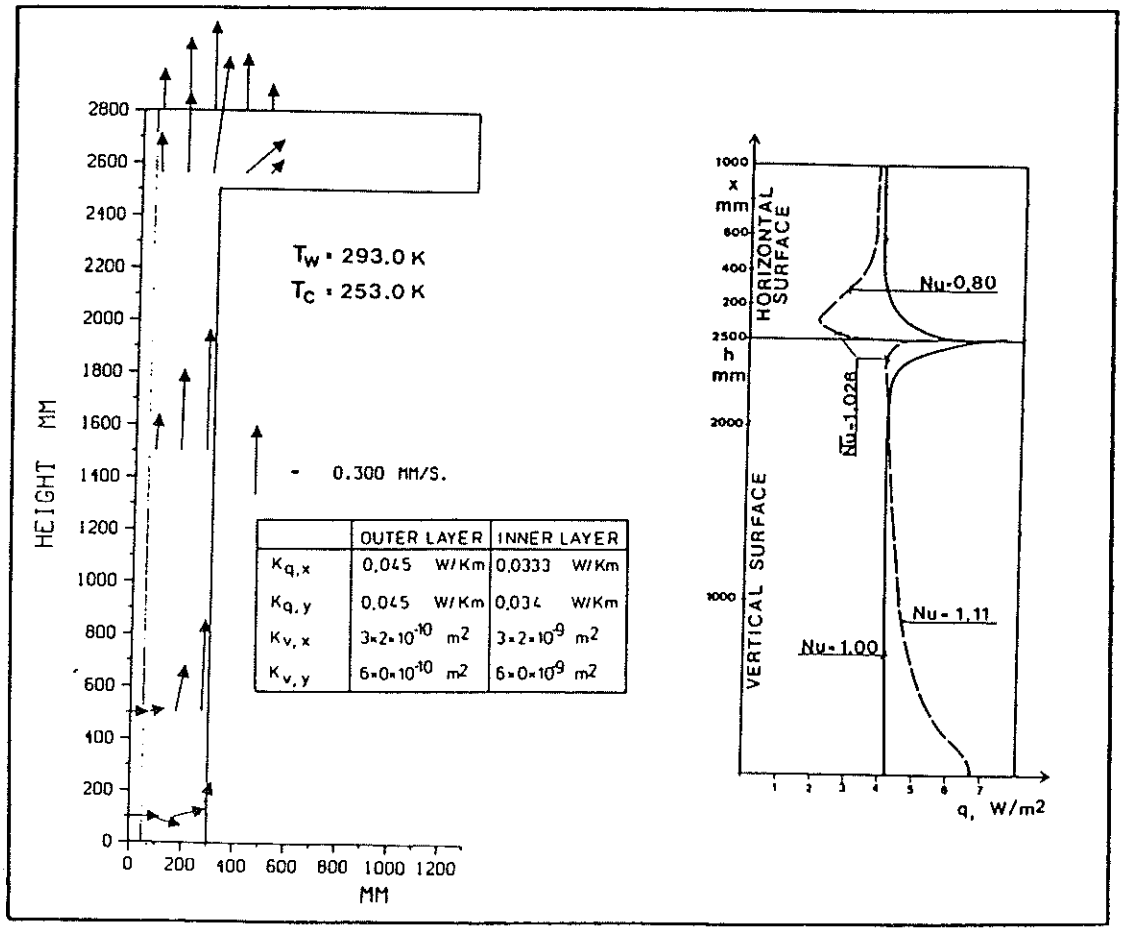

Figure 9. Calculated flow field and heat flux profiles for an L-shaped structure with permeable cold surface

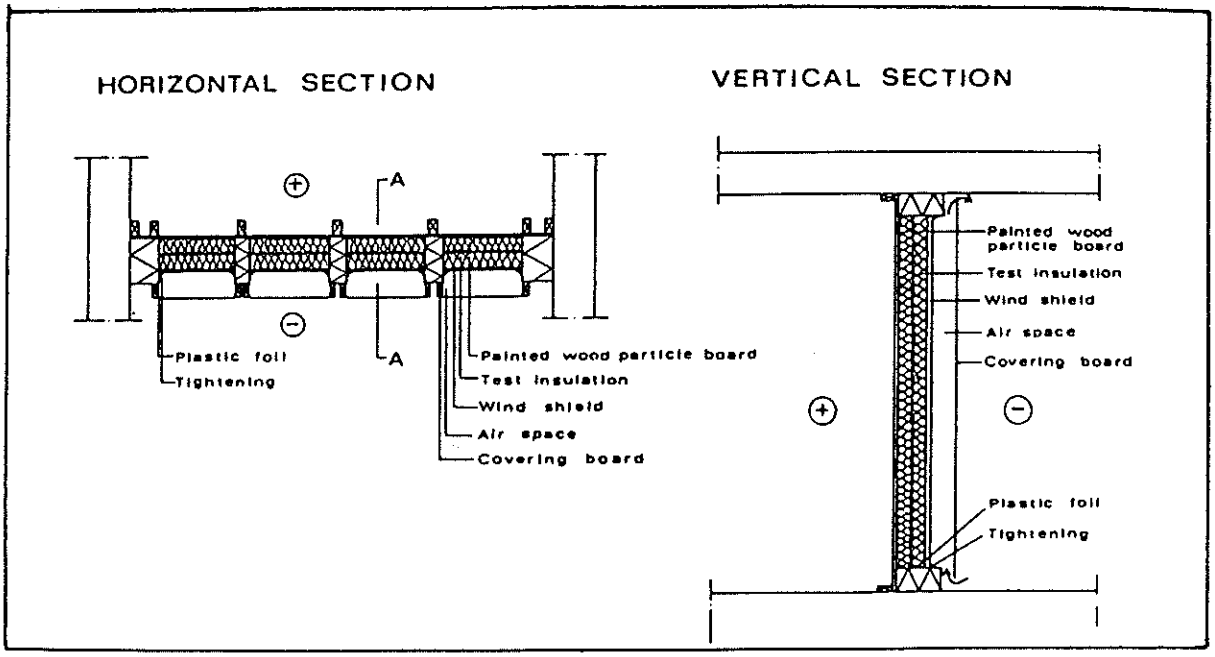

Figure 10. Horizontal and vertical sections of test walls

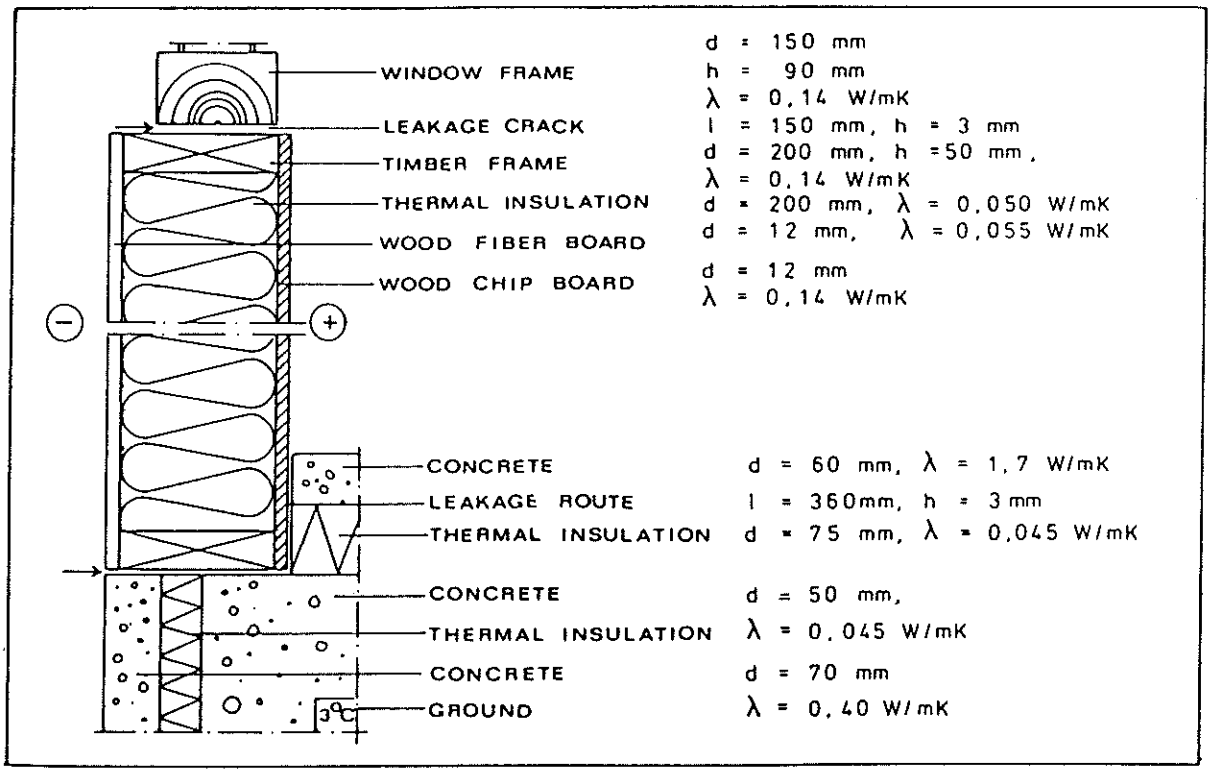

Figure 11. Wall structure in simulation and material properties

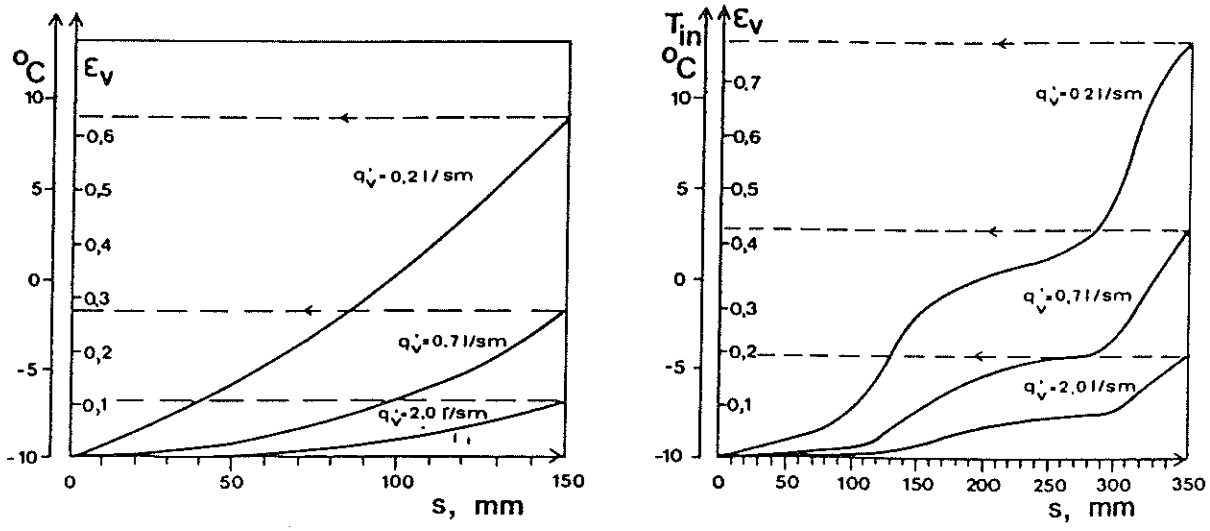

Figure 12. Warming up of leakage air in a crack between window frame and wall (left) and between wood wall and foundation (right)

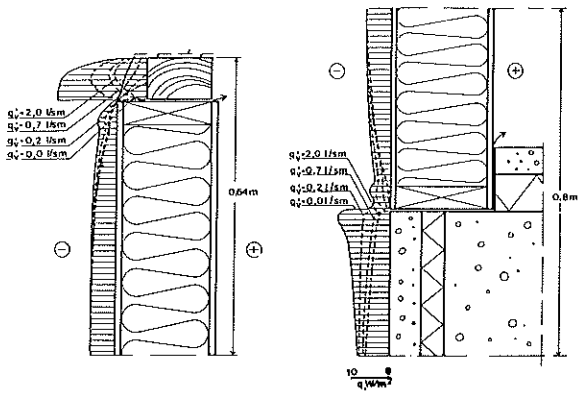

Figure 13. Heat flux profiles at outer surfaces of structures

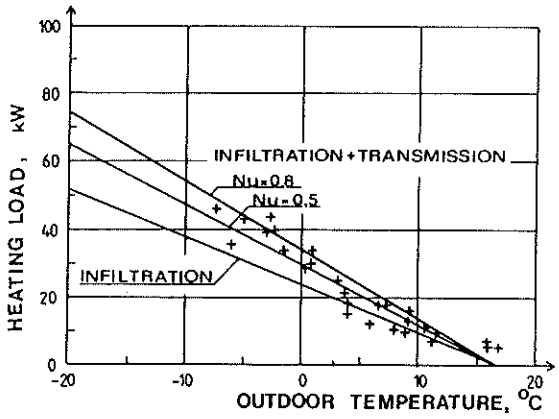

Figure 14. Measured and calculated heating load of a building

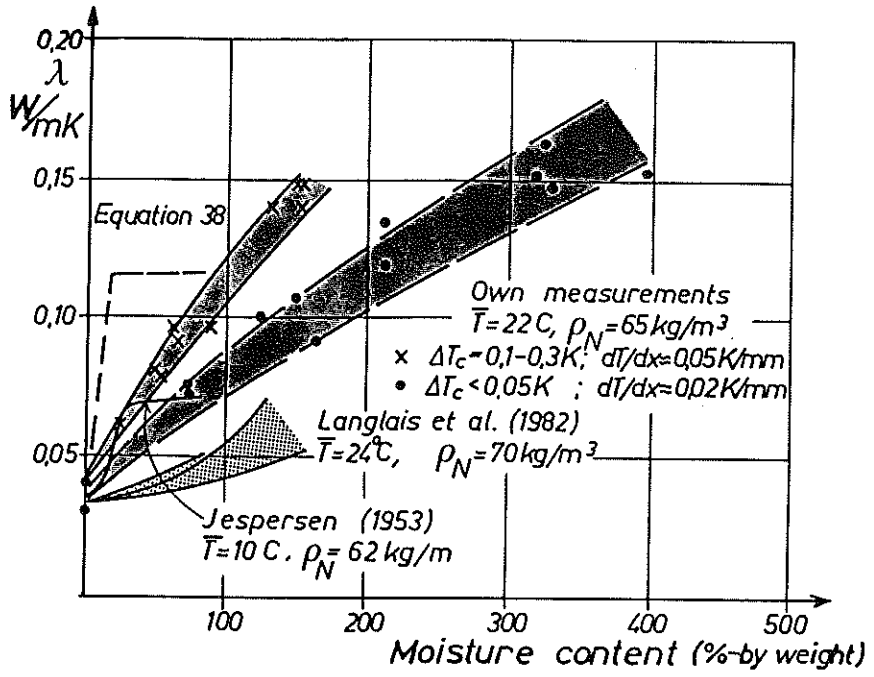

Figure 15. Thermal conductivities of moist fibrous insulants

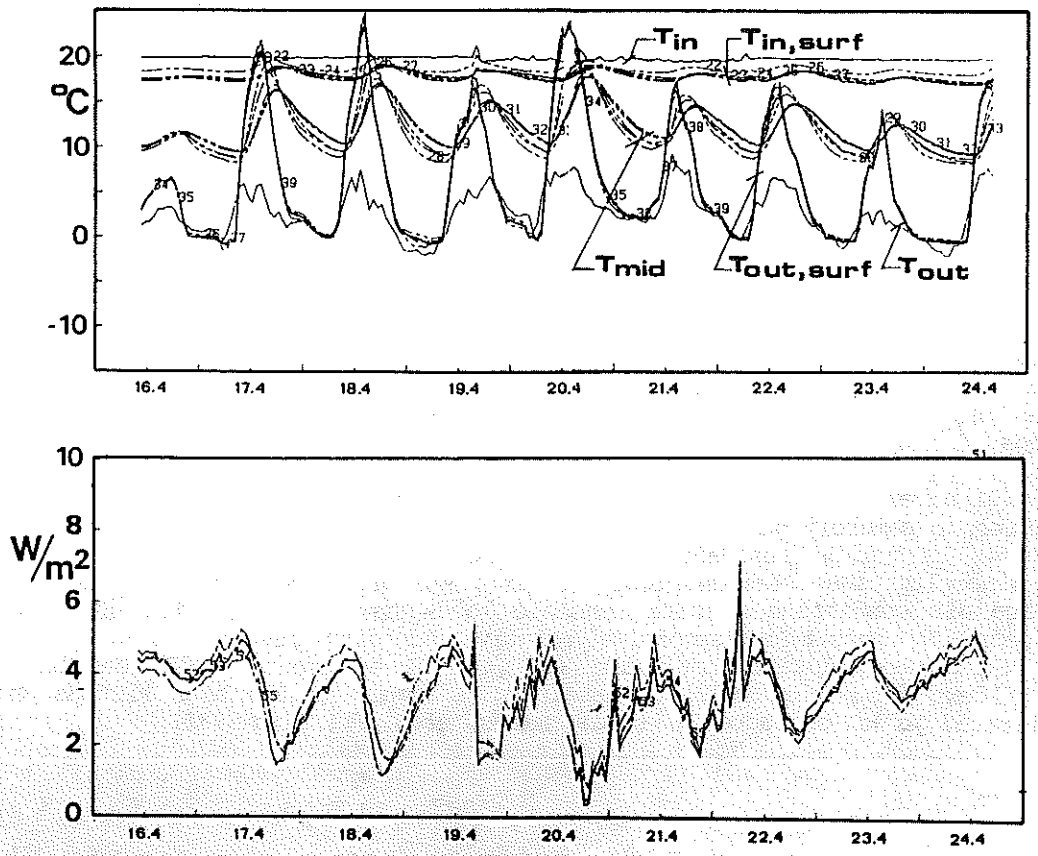

Figure 16. Measured temperature and heat flux distributions in a flat roof with 220-mm-thick glass fiber insulation